Steady Infiltration into Two-Layered Soils with a Root-Water Uptake

Imam Solekhudin, Sumardi, and Zenith Purisha

Abstract—**This paper investigates steady infiltration problems involving periodic channels in two-layered soil with the presence of root-water uptake. The problems are governed by a set of Richards' equations accompanied by boundary interface conditions. To address these problems, we transform the system of Richards' equations, along with the corresponding boundary conditions, into a set of steady diffusion-convection equations with transformed boundary conditions. The mathematical model is then tackled through a numerical approach utilizing the Iterative Dual Reciprocity Method (IDRM). Through this numerical method, we obtain solutions that describe the distribution of soil water potential and hydraulic conductivity within the soil. The outcomes of this study shed light on the influence of soil texture and saturated hydraulic conductivity on the values of soil water potential and hydraulic conductivity.**

Index Terms—**Steady infiltration, layered soil, iterative dual reciprocity method, root-water uptake.**

I. Introduction

THe examination of water infiltration through layered soils is a fundamental aspect of soil physics. This line of research appears to have originated from investigations conducted in rice fields, where a saturated zone was maintained above an unsaturated zone within a soil structure featuring fine soil overlying coarse soil [1]. Consequently, this initial work has spurred a series of studies focused on water infiltration through layered soils, encompassing scenarios with fine-over-coarse or coarse-over-fine soil structures. These studies have taken various forms, including analytical investigations [2], [3], [4], numerical simulations [5], [6], and experimental research [7].

Srivastava and Yeh conducted analytical studies on problems related to transient infiltration toward the water table, focusing on both homogeneous and layered soils [2]. However, their proposed method may not be suitable for solving infiltration issues in layered soils with varying soil coarseness. To address this limitation, Barontini et al. introduced an analytical method to handle infiltration problems where hydraulic conductivity decreases exponentially with depth [3]. Nevertheless, the approach employed by Barontini et al. is not applicable when the hydraulic conductivity in the lower layer exceeds that in the upper layer. To fill this gap, De Luca and Cepeda proposed an analytical approach capable of addressing one-dimensional infiltration into two-layered soils of any type [4].

In addition to analytical approaches, finite difference methods (FDM) have been utilized to investigate one-dimensional flow in layered soils. Ross and Bristow, for instance, employed FDM for simulating one-dimensional water movement in layered soils [6]. Oldenburg and Pruess worked on the study of a capillary barrier that forms at the interface of a fine soil layer overlying a coarse soil layer using FDM [5].

Numerical techniques extensively employed for solving the Richards equation in multi-layered soil problems include finite element methods (FEM). Researchers have applied FEM in various studies, as evidenced by references such as [8], [9], [10], [11], [12], [13], [14], [15], [16]. In practice, two commercial models, namely HYDRUS and SEEP/W, are commonly used to tackle these problems. These models typically rely on a Galerkin approach to finite elements, which makes them well-suited for addressing challenges in flow domains with complex geometries. However, it's worth noting that these methods come with certain drawbacks. Specifically, across interfaces between elements, the normal flux often exhibits discontinuities, and mass is not conserved within element [17], [18], [19].

In recent times, the boundary element method (BEM) and the dual reciprocity method (DRM) have gained increased attention among scientists and engineers in the realm of numerical methods. They offer distinct advantages over finite element methods (FEM) and finite difference methods (FDM). Notably, one of their key advantages is their ability to reduce problem dimension by one and enable solution evaluation at any point within the problem domain, as referenced in works such as [20], [21].

Both BEM and DRM have been effectively employed by numerous researchers to address infiltration problems in homogeneous soils, as demonstrated in studies by researchers [22], [23], [24], [25], [26], [27]. To implement BEM, it is necessary to derive the fundamental solution of the governing equation for the specific problem at hand. For infiltration problems, this entails obtaining the fundamental solution of either the Helmholtz equation or the diffusion-convection equation.

In contrast, DRM does not require such complex fundamental solutions. It relies on a simpler fundamental solution, typically that of Laplace's equation. Moreover, DRM is adaptable to solving infiltration problems even when root-water uptake is involved, whereas BEM may not be suitable for such scenarios. This highlights the flexibility of DRM compared to BEM as a numerical method for tackling a wide range of infiltration problems.

The majority of previous studies on water flow through

Manuscript received September 12, 2023; revised February 29, 2024.

This work was supported by the Directorate of Higher Education of the Government of Republic Indonesia under Fundamental Research Grant with contract number 122/E5/PG.02.00.PL/2023; 3156/UN1/DITLIT/Dit-Lit/PT.01.03/2023.

Imam Solekhudin is a Professor at Department of Mathematics, Faculty of Mathematics and Natural Sciences, Universitas Gadjah Mada, Yogyakarta, 55281 Indonesia. (corresponding author, phone: 62-274-552243; e-mail: imams@ugm.ac.id.)

Sumardi is an Associate Professor at Department of Mathematics, Faculty of Mathematics and Natural Sciences, Universitas Gadjah Mada, Yogyakarta, 55281 Indonesia. (e-mail: mardimath@ugm.ac.id.)

Zenith Purisha is an Assistant Professor at Department of Mathematics, Faculty of Mathematics and Natural Sciences, Universitas Gadjah Mada, Yogyakarta, 55281 Indonesia. (e-mail: zenith.purisha@ugm.ac.id.)

layered soils have primarily focused on one-dimensional problems. Consequently, the objective of this study is to develop a mathematical model for simulating two-dimensional water infiltration scenarios in two-layered soils, accounting for root-water uptake. This research builds upon the work presented in a prior study [28].

In this paper, we introduce an Iterative Dual Reciprocity Method (IDRM) as a novel approach to solve the formulated model. By employing this method, we have the capability to transform the model into a one-dimensional problem, simplifying the computational process. Addressing the nonlinearity of the boundary conditions at the interface involves implementing iterative steps within the IDRM framework. Our application of the IDRM will be focused on solving water infiltration problems originating from periodic trapezoidal channels into two-layered soils that incorporate root-water uptake. The ultimate goal is to simulate the suction potential and hydraulic conductivity profiles within the soil.

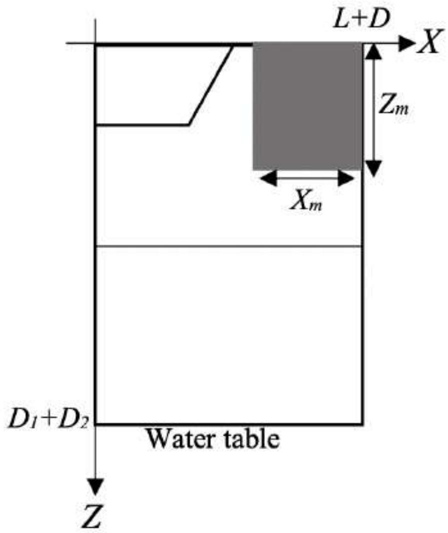

Fig. 1: Geometry of the problems.

II. Problem formulation

In this research, we examine problems related to steady infiltration problems from periodic trapezoidal channels in two-layered soils. These channels have the surface area of $2L$ per unit length of the channels, with the distance between the centers of adjacent channels measuring $2(L+D)$. The channels possess a width of $4L/\pi$ and a depth of $3L/2\pi$. The upper layer contains a root zone, characterized by dimensions of $2X_m$ for width and Z_m for depth. These channels remain continuously filled with water, and water infiltrates the soil at a constant rate, denoted as v_0. We make certain assumptions in line with previous works [29], [23], [24], which consider the channels to be sufficiently long and numerous. Additionally, we assume that the channels' geometry remains unchanged in the direction parallel to their length.

The upper layer has a thickness of D_1, while the lower layer extends to a depth of D_2 above the water table. Consequently, the problems we address can be treated as two-dimensional problems. Since the problem is symmetrical about the center of each channel and any line located at a distance of $L+D$ from the channel's center, we can represent the problem's geometry using a Cartesian coordinate system denoted as XOZ. This coordinate system is bounded by the lines $X=0$, $X=L+D$, $Z=0$, and $Z=D_1+D_2$. It's important to note that in this coordinate system, the positive direction for the Z axis is downward. The problem's geometry is further visualized in Figure 1.

III. Basic equations

A. Mathematical model development

Water infiltration in unsaturated soil with sink term is modelled by the Richards' equation [30], [31], [32], [33], [34], given by

$$\frac{\partial \theta}{\partial t} = \nabla.\left(K\nabla\psi\right) - \frac{\partial K}{\partial Z} - S, \tag{1}$$

which can be written as

$$\frac{\partial \theta}{\partial t} = \frac{\partial}{\partial X}\left(K\frac{\partial \psi}{\partial X}\right) + \frac{\partial}{\partial Z}\left(K\frac{\partial \psi}{\partial Z}\right) - \frac{\partial K}{\partial Z} - S, \tag{2}$$

where θ, K and S are respectively the water content in the soil, the hydraulic conductivity in the soil [35], [36], [37], [38], and the sink term. Here ψ is the suction potential [39], [40], [23], [41], [30]. The sink term in this study is the root water uptake, modeled as that in [26],

$$S(X,Z,\psi) = \gamma(\psi)\frac{L_t\beta(X,Z)T_{pot}}{\int\limits_0^{Z_m}\int\limits_{L+D-X_m}^{L+D}\beta(X,Z)dXdZ}, \tag{3}$$

where γ is the dimensionless soil water stress response function, defined as [24]

$$\gamma(\psi) = \begin{cases} -\frac{5}{8}\psi, & \text{for } -1.6 \leq \psi \leq 0 \\ 1, & \text{for } -4.7 < \psi < -1.6 \\ \frac{2}{7}\psi + \frac{82}{35}, & \text{for } -8.2 \leq \psi \leq -4.7 \end{cases}, \tag{4}$$

L_t is the width of the soil surface associated with the transpiration rate, T_{pot} is the potential transpiration, and β is the spatial root-water uptake distribution modeled as

$$\beta(X,Z) = \left(1 - \frac{Z}{Z_m}\right)\left(1 - \frac{L+D-X}{X_m}\right)\exp(-K), \tag{5}$$

where

$$K = \frac{P_Z}{Z_m}|Z^* - Z| + \frac{P_X}{X_m}|X^* - (L+D-X)|.$$

Here P_Z, P_X, Z^* and X^* are empirical parameters.

Flux normal to a surface with outward pointing normal $\mathbf{n} = (n_1, n_2)$ is [30]

$$F = Un_1 + Vn_2 = -K\left[\frac{\partial \psi}{\partial X}n_1 + \left(\frac{\partial \psi}{\partial Z} - 1\right)n_2\right]. \tag{6}$$

Applying Gardner's formula [42], [43],

$$K = K_s e^{\alpha\psi}, \tag{7}$$

where K_s is the saturated hydraulic conductivity and α is the soil parameter related to the soil grain size, we have

$$\frac{\partial \psi}{\partial X} = \frac{1}{\alpha K}\frac{\partial K}{\partial X}, \tag{8}$$

$$\frac{\partial \psi}{\partial Z} = \frac{1}{\alpha K}\frac{\partial K}{\partial Z}, \tag{9}$$

and Equation (2) becomes

$$\frac{\partial\theta}{\partial t} = \frac{1}{\alpha}\left(\frac{\partial^2 K}{\partial X^2} + \frac{\partial^2 K}{\partial Z^2}\right) - \frac{\partial K}{\partial Z} - S. \tag{10}$$

Flux normal in Equation (6) can now be written as

$$F = \left(-\frac{1}{\alpha}\frac{\partial K}{\partial X}\right) n_1 + \left(K - \frac{1}{\alpha}\frac{\partial K}{\partial Z}\right) n_2. \tag{11}$$

For the case of time-independent infiltration problem, Equation (10) becomes

$$\frac{\partial^2 K}{\partial X^2} + \frac{\partial^2 K}{\partial Z^2} - \alpha\frac{\partial K}{\partial Z} = S. \tag{12}$$

In this study, time-independent infiltration problems into two-layered soil with root-water uptake in the upper layer is considered. Following [4], the system of differential equations to model the problems is

$$\frac{\partial^2 K_1}{\partial X^2} + \frac{\partial^2 K_1}{\partial Z^2} - \alpha_1\frac{\partial K_1}{\partial Z} = \alpha_1 S, \tag{13}$$

$$\frac{\partial^2 K_2}{\partial X^2} + \frac{\partial^2 K_2}{\partial Z^2} - \alpha_2\frac{\partial K_2}{\partial Z} = 0, \tag{14}$$

where K_1 and α_1 are, respectively, the hydraulic conductivity and the soil parameter of the upper layer, K_2 and α_2 are the hydraulic conductivity and the soil parameter of the lower layer. Flux normal to the upper layer and the lower layer with outward pointing pointing normals $\mathbf{n}_1 = (n_{11}, n_{21})$ and $\mathbf{n}_2 = (n_{12}, n_{22})$ are

$$F_1 = \left(-\frac{1}{\alpha_1}\frac{\partial K_1}{\partial X}\right) n_{11} + \left(K_1 - \frac{1}{\alpha_1}\frac{\partial K_1}{\partial Z}\right) n_{21}, \tag{15}$$

$$F_2 = \left(-\frac{1}{\alpha_2}\frac{\partial K_2}{\partial X}\right) n_{12} + \left(K_2 - \frac{1}{\alpha_2}\frac{\partial K_2}{\partial Z}\right) n_{22}, \tag{16}$$

respectively.

1) Interface conditions: The conditions at the interface layer are given by [4], [19]

$$\psi_1 = \psi_2, \tag{17}$$

$$F_1 = -F_2, \tag{18}$$

at $Z = D_1$. Here ψ_1 is the soil water potential in the upper layer, and ψ_2 is the soil water potential in the lower layer.

From Equation (7), we have

$$\psi_i = \frac{1}{\alpha_i}\ln\left(\frac{K_i}{K_{si}}\right), i = 1, 2. \tag{19}$$

Use of Equation (19) in Equation (17) yields

$$K_2 = \frac{K_{s2}}{K_{s1}^{\alpha_2/\alpha_1}} K_1^{\alpha_2/\alpha_1}, \tag{20}$$

where K_{s1} is the saturated hydraulic conductivity of upper level soil and K_{s2} is the saturated hydraulic conductivity of lower level soil.

Substituting Equation (20) into Equation (16) results in

$$F_2 = \left(-\frac{1}{\alpha_2}\frac{\partial K_2}{\partial X}\right) n_{12} + \left(\frac{K_{s2}}{K_{s1}^{\alpha_2/\alpha_1}} K_1^{\alpha_2/\alpha_1} - \frac{1}{\alpha_2}\frac{\partial K_2}{\partial Z}\right) n_{22}, \tag{21}$$

Substituting Equation (15) and Equation (21) to Equation (18) yields

$$\frac{\partial K_2}{\partial n} = \alpha_2\left(K_1 - \frac{K_{s2}}{K_{s1}^{\alpha_2/\alpha_1}} K_1^{\alpha_2/\alpha_1}\right) - \frac{\alpha_2}{\alpha_1}\frac{\partial K_1}{\partial n}. \tag{22}$$

2) Boundary conditions: From the boundary conditions described in the preceding section and the interface conditions presented, using Equation (15) and Equation (16), boundary interface conditions in terms of K_1 and K_2 are

$$\frac{\partial K_1}{\partial n} = \alpha_1(v_0 + n_{21}K_1), \text{ on the surface of the channel,} \tag{23}$$

$$\frac{\partial K_1}{\partial n} = -\alpha_1 K_1, \text{ for } \frac{2L}{\pi} < X < L + D \text{ and } Z = 0, \tag{24}$$

$$\frac{\partial K_1}{\partial n} = 0, \text{ for } X = 0 \text{ and } \frac{3L}{2\pi} < Z < D_1, \tag{25}$$

$$\frac{\partial K_1}{\partial n} = 0, \text{ for } X = L + D \text{ and } 0 < Z < D_1, \tag{26}$$

$$K_2 = \frac{K_{s2}}{K_{s1}^{\alpha_2/\alpha_1}} K_1^{\alpha_2/\alpha_1}, \text{ for } 0 < X < L + D \text{ and } Z = D_1, \tag{27}$$

$$\frac{\partial K_2}{\partial n} = \alpha_2\left(K_1 - \frac{K_{s2}}{K_{s1}^{\alpha_2/\alpha_1}} K_1^{\alpha_2/\alpha_1}\right) - \frac{\alpha_2}{\alpha_1}\frac{\partial K_1}{\partial n}, \text{ for } 0 < X < L + D \text{ and } Z = D_1, \tag{28}$$

$$\frac{\partial K_2}{\partial n} = 0, \text{ for } X = 0 \text{ and } D_1 < Z < D_1 + D_2, \tag{29}$$

$$\frac{\partial K_2}{\partial n} = 0, \text{ for } X = L + D \text{ and } D_1 < Z < D_1 + D_2, \tag{30}$$

and

$$K_2 = K_{s2}, \text{ for } 0 < X < L + D \text{ and } Z = D_1 + D_2. \tag{31}$$

Hence, the mathematical model for two-layered infiltration problems in present study is the system of partial differential equations (13) and (14) with respect to boundary interface conditions (23) to (31).

B. Dual reciprocity procedure

Equations (13) and (14) are two-dimensional diffusion-convection equations, which may be solved numerically using a DRM by recasting the equations into

$$\begin{aligned}\lambda(\xi_1, \eta_1)K_1(\xi_1, \eta_1) &= \alpha_1 \iint_{\Omega_1} \varphi(x, y; \xi_1, \eta_1) \\ &\quad \times \left[\frac{\partial}{\partial Z}(K_1(x, y)) + S(\psi, X, Z)\right] dxdy \\ &\quad + \int_{\Gamma_1} \left[K_1(x, y)\frac{\partial}{\partial n}(\varphi(x, y; \xi_1, \eta_1)) \right. \\ &\quad \left. - \varphi(x, y; \xi_1, \eta_1)\frac{\partial}{\partial n}(K_1(x, y))\right] ds,\end{aligned} \tag{32}$$

and

$$\begin{aligned}\lambda(\xi_2, \eta_2)K_2(\xi_2, \eta_2) &= \alpha_2 \iint_{\Omega_2} \varphi(x, y; \xi_2, \eta_2)\frac{\partial}{\partial Z}(K_2(x, y))dxdy \\ &\quad + \int_{\Gamma_2} \left[K_2(x, y)\frac{\partial}{\partial n}(\varphi(x, y; \xi_2, \eta_2)) \right. \\ &\quad \left. - \varphi(x, y; \xi_2, \eta_2)\frac{\partial}{\partial n}(K_2(x, y))\right] ds,\end{aligned} \tag{33}$$

where $\varphi(x,y;\xi,\eta)$ is the fundamental solution of two-dimensional Laplace equation, and

$$\lambda(\xi_i,\eta_i) = \begin{cases} 1/2, \ (\xi_i,\eta_i) \text{ lies on smooth part of } \Gamma_i \\ 1, \ (\xi_i,\eta_i) \in \Omega_i \end{cases}, \quad \text{for } i=1,2. \tag{34}$$

Boundaries Γ_1 and Γ_2 are discretized into a number of elements, and a number of interior points are chosen in Ω_1 and Ω_2. Let $C_1^{(1)}$, $C_1^{(2)}$, $\cdots$, $C_1^{(N_1)}$ be the line segments on Γ_1 ($\Gamma_1 \approx C_1^{(1)} \cup C_1^{(2)} \cup \cdots \cup C_1^{(N_1)}$), and $C_2^{(1)}$, $C_2^{(2)}$, $\cdots$, $C_2^{(N_2)}$ be the line segments on Γ_2 ($\Gamma_2 \approx C_2^{(1)} \cup C_2^{(2)} \cup \cdots \cup C_2^{(N_2)}$). Point $(a_1^{(i)}, b_1^{(i)})$ is the mid point of $C_1^{(i)}$, $i=1,2,\cdots,N_1$, and Point $(a_2^{(j)}, b_2^{(j)})$ is the mid point of $C_2^{(j)}$, $j=1,2,\cdots,N_2$. Let $(a_1^{(N_1+1)}, b_1^{(N_1+1)})$, $(a_1^{(N_1+2)}, b_1^{(N_1+1)})$, $\cdots$, $(a_1^{(N_1+M_1)}, b_1^{(N_1+M_1)})$ be the interior points in Ω_1, and $(a_2^{(N_2+1)}, b_2^{(N_2+1)})$, $(a_2^{(N_2+2)}, b_2^{(N_2+1)})$, $\cdots$, $(a_2^{(N_2+M_2)}, b_2^{(N_2+M_2)})$ be the interior points in Ω_2. Let n_0 be the number of elements on the interface.

Using the elements and interior points described, the integral equations in Equations (32) and (33) are recast into a system of linear algebraic equations

$$\begin{aligned} \lambda^{(n_1)} K_1^{(n_1)} &= \sum_{j=1}^{N_1} \left(\mathfrak{F}_{2,1}^{(n_1 j)} K_1^{(j)} - \mathfrak{F}_{1,1}^{(n_1 j)} \bar{K}_1^{(j)} \right) \\ &\quad + \alpha_1 \sum_{j=1}^{N_1+M_1} {\mu_1}^{(n_1 j)} \left[S\left(K_1^{(i)}, a_1^{(i)}, b_1^{(i)} \right) \right. \\ &\quad \left. + \sum_{m=1}^{N_1+M_1} \bar{\rho}_Z^{(jm)} \left(\sum_{i=1}^{N_1+M_1} \omega_1^{(mi)} K_1^{(i)} \right) \right], \\ &\text{for } n_1 = 1,2,\cdots,N_1+M_1, \end{aligned} \tag{35}$$

and

$$\begin{aligned} \lambda^{(n_2)} K_2^{(n_2)} &= \sum_{k=1}^{N_2} \left(\mathfrak{F}_{2,2}^{(n_2 k)} K_2^{(k)} - \mathfrak{F}_{1,2}^{(n_2 k)} \bar{K}_2^{(k)} \right) \\ &\quad + \alpha_2 \sum_{k=1}^{N_2+M_2} {\mu_2}^{(n_2 k)} \\ &\quad \times \left[\sum_{l=1}^{N_2+M_2} \bar{\rho}_Z^{(kl)} \left(\sum_{i=1}^{N_2+M_2} \omega_2^{(li)} K_2^{(i)} \right) \right], \\ &\text{for } n_2 = 1,2,\cdots,N_2+M_2. \end{aligned} \tag{36}$$

In system of linear algebraic equations (35) and (36), the symbols used for notation are as follows: $\lambda^{(n_1)} = \lambda({a_1}^{(n_1)}, {b_1}^{(n_1)})$, $\lambda^{(n_2)} = ({a_2}^{(n_2)}, {b_2}^{(n_2)})$, $K_1^{(n_1)} = K_1({a_1}^{(n_1)}, {b_1}^{(n_1)})$, $K_2^{(n_2)} = K_2({a_2}^{(n_2)}, {b_2}^{(n_2)})$, $\bar{K_1}^{(n_1)} = (\partial K_1/\partial n)|_{(x,y)=({a_1}^{(n_1)}, {b_1}^{(n_1)})}$, $\bar{K_2}^{(n_2)} = (\partial K_2/\partial n)|_{(x,y)=({a_2}^{(n_2)}, {b_2}^{(n_2)})}$,

$$\begin{aligned} \mathfrak{F}_{1,1}^{(n_1 j)} &= \int_{C_1^{(j)}} \varphi(x,y;a_1^{(n_1)}, b_1^{(n_1)}) ds(x,y), \\ \mathfrak{F}_{1,2}^{(n_2 j)} &= \int_{C_2^{(j)}} \varphi(x,y;a_2^{(n_2)}, b_2^{(n_2)}) ds(x,y), \\ \mathfrak{F}_{2,1}^{(n_1 j)} &= \int_{C_1^{(j)}} \frac{\partial}{\partial n} \left[\varphi(x,y;a_1^{(n_1)}, b_1^{(n_1)}) \right] ds(x,y), \\ \mathfrak{F}_{2,2}^{(n_2 j)} &= \int_{C_2^{(j)}} \frac{\partial}{\partial n} \left[\varphi(x,y;a_2^{(n_2)}, b_2^{(n_2)}) \right] ds(x,y). \end{aligned}$$

The notation $\rho^{(mk)}$ represents the value of a radial basis function ρ centered at the point $(a^{(m)}, b^{(m)})$ when evaluated at the point $(a^{(k)}, b^{(k)})$. The symbol $\bar{\rho}_Z^{(jm)}$ denotes the partial derivative of ρ with respect to Z when evaluated at the point $(a^{(m)}, b^{(m)})$, where ρ is the radial basis function centered about the point $(a^{(j)}, b^{(j)})$. The coefficients ${\omega_1}^{(mk)}$ and ${\omega_2}^{(nk)}$ are defined as

$$\begin{aligned} \sum_{i=1}^{N_1+L_1} {\omega_1}^{(mi)} \rho^{(ik)} &= \begin{cases} 1, & \text{if } m=k \\ 0, & \text{if } m \neq k \end{cases}, \\ \sum_{i=1}^{N_2+L_2} {\omega_2}^{(ni)} \rho^{(ik)} &= \begin{cases} 1, & \text{if } n=k \\ 0, & \text{if } n \neq k \end{cases}. \end{aligned}$$

Two numbers ${\mu_1}^{(n_1 j)}$ and ${\mu_2}^{(n_2 j)}$ are defined as

$$\begin{aligned} {\mu_1}^{(n_1 j)} &= \sum_{k=1}^{N_1+L_1} {\Psi_1}^{(n_1 k)} {\omega_1}^{(kj)}, \\ \text{and } {\mu_2}^{(n_2 j)} &= \sum_{k=1}^{N_2+L_2} {\Psi_2}^{(n_2 k)} {\omega_2}^{(kj)}, \end{aligned}$$

where

$$\begin{aligned} {\Psi_1}^{(n_1 k)} &= \lambda^{(n_1)} \chi(a_1^{(n_1)}, b_1^{(n_1)}, a_1^{(k)}, b_1^{(k)}) \\ &\quad + \sum_{j=1}^{N_1} \left[\frac{\partial}{\partial n} \left(\chi(x,y;{a_1}^{(j)}, {b_1}^{(j)}) \right) \right] \Big|_{(x,y)=({a_1}^{(k)}, {b_1}^{(k)})} \\ &\qquad \times \mathfrak{F}_{1,1}^{(nj)} \\ &\quad - \sum_{j=1}^{N} \chi({a_1}^{(k)}, {b_1}^{(k)}; {a_1}^{(j)}, {b_1}^{(j)}) \mathfrak{F}_{2,1}^{(nj)}, \end{aligned}$$

$$\begin{aligned} {\Psi_2}^{(n_2 k)} &= \lambda^{(n_2)} \chi(a_2^{(n_2)}, b_2^{(n_2)}, a_2^{(k)}, b_2^{(k)}) \\ &\quad + \sum_{j=1}^{N_2} \left[\frac{\partial}{\partial n} \left(\chi(x,y;{a_2}^{(j)}, {b_2}^{(j)}) \right) \right] \Big|_{(x,y)=({a_2}^{(k)}, {b_2}^{(k)})} \\ &\qquad \times \mathfrak{F}_{1,2}^{(nj)} \\ &\quad - \sum_{j=1}^{N} \chi({a_1}^{(k)}, {b_1}^{(k)}; {a_1}^{(j)}, {b_1}^{(j)}) \mathfrak{F}_{2,2}^{(nj)}, \end{aligned}$$

and χ is a function satisfying

$$\frac{\partial^2 \chi}{\partial x^2} + \frac{\partial^2 \chi}{\partial y^2} = \rho.$$

In system of linear algebraic equations (35), when j ranges from N_0+1 to N_0+n_0, both K_1 and $\bar{K_1}$ are unknown variables. Consequently, the total number of unknowns are $N_1 + M_1 + n_0$. Similarly, the number of unknowns in system of linear algebraic equation (36) is $N_2 + M_2 + n_0$. Consequently, it may not be feasible to solve the system of linear algebraic equations represented by (35) and (36) since the number of equations provided is $N_1 + M_1$ and $N_2 + M_2$. To address this, we apply interface conditions (20) and (22) so that the system of linear algebraic equations (36) can be expressed as follows.

$$
\begin{aligned}
&\lambda^{(n_2)}\kappa^{(n_2)}\\
&= \sum_{j=1}^{n_0}\Bigg\{\mathfrak{F}_{2,2}^{(n_2 j)}\frac{K_{s2}}{K_{s1}^{\alpha_2/\alpha_1}}\left[K_1^{(N_0+n_0+1-j)}\right]^{\alpha_2/\alpha_1}\\
&\qquad -\mathfrak{F}_{1,2}^{(n_2 j)}\Bigg[\alpha_2\Bigg(K_1^{(N_0+n_0+1-j)}-\frac{K_{s2}}{K_{s1}^{\alpha_2/\alpha_1}}\\
&\qquad\qquad \times\left[K_1^{(N_0+n_0+1-j)}\right]^{\alpha_2/\alpha_1}\Bigg)\\
&\qquad\qquad -\frac{\alpha_2}{\alpha_1}\bar{K}_1^{(N_0+n_0+1-j)}\Bigg]\Bigg\}\\
&\quad +\sum_{j=n_0+1}^{N_2}\left(\mathfrak{F}_{2,2}^{(n_2 j)}K_2^{(j)}-\mathfrak{F}_{1,2}^{(n_2 j)}\bar{K}_2^{(j)}\right)\\
&\quad +\alpha_2\sum_{j=1}^{n_0}\mu^{(n_2 j)}\left[\sum_{m=1}^{N_2+M_2}\bar{\rho}_Z^{(jm)}\left(\sum_{i=1}^{n_0}\omega_2^{(mi)}\frac{K_{s2}}{K_{s1}^{\alpha_2/\alpha_1}}\right.\right.\\
&\qquad\qquad \left.\left.\times\left[K_1^{(N_0+n_0+1-i)}\right]^{\alpha_2/\alpha_1}\right)\right],\\
&\quad +\alpha_2\sum_{j=n_0+1}^{N_2+M_2}\mu^{(n_2 j)}\\
&\qquad \times\left[\sum_{m=1}^{N_2+M_2}\bar{\rho}_Z^{(jm)}\left(\sum_{i=n_0+1}^{N_2+M_2}\omega_2^{(mi)}K_2^{(i)}\right)\right],
\end{aligned}
$$

for $n_2 = 1, 2, \cdots, N_2 + M_2$. (37)

It can be seen that (37) is not a system of linear algebraic equations. Here

$$
\kappa^{(n_2)} = \begin{cases} K^*\left[K_1^{(N_0+n_0+1-n_2)}\right]^{\alpha}, \text{ for } n_2 = 1, 2, ..., n_0 \\ K_2^{(n_2)}, \text{ for } n_2 = n_0+1, n_0+2, ..., N_2+M_2 \end{cases},
$$

where $\alpha = \alpha_2/\alpha_1$ and $K^* = K_{s2}/(K_{s1})^{\alpha}$.

Now, the number of unknowns in system of linear algebraic equations (35) and system of algebraic equations (37) is $N_1 + N_2 + M_1 + M_2$, as well as the number of equations. Hence, solutions may be obtained by solving these system of algebraic equations simultaneously. Since the system of algebraic equations (37) is not a system of linear algebraic equation, hence we need to transform (37) into a system of linear algebraic equations using the iterative steps as those in [28].

IV. RESULTS AND DISCUSSION

In this section, the DRM described in Subsection III-B is applied to solve steady infiltration problems from periodic trapezoidal channels in two-layered soils with root-water uptake. As that in the previous study, the fluxes on the surface of the channels are assumed to be constant, v_0. We set the constant v_0 as

$$
v_0 = 0.75 \times 0.099 \text{ m/day}, \tag{38}
$$

where 0.099 m/day is the saturated hydraulic conductivity of Pima Clay Loam. This value of v_0 is chosen in a similar way as that in [44]. We set $\varepsilon = 10^{-4}$. There are three different types of soil involved in this study, Pima Clay Loam (PCL), Guelph Loam (GL), and Touchet Silt Loam (TSL). Values of K_s and α of the soils are summarized in Table I.

TABLE I: Soil's parameters.

	PCL	GL	TSL
K_s (m/day)	0.099	0.3171	0.4199
α (m^{-1})	1.4	3.4	1.56

The values of the saturated hydraulic conductivity, K_s, and the soil parameter, α, used in this paper are as those reported by Amozegar-Fard et al. [45], and Bresler [46]. For the root-water uptake function, the depth and the width of the root zone, and other parameters are adopted from one of those proposed in [47], sumarized in Table II.

TABLE II: Parameters of root-water uptake function.

X_m (m)	Z_m (m)	L_t (m)	T_{pot} (m/day)
0.5	1.0	0.5	0.004
P_Z	P_X	Z^* (m)	X^* (m)
1.0	1.0	0.2	1.0

The numerical method described is then implemented to solve four different cases. The four different cases are PCL-GL, GL-PCL, PCL-TSL, and TSL-GL, with the depth of the upper and the lower layer are 2 m and 3 m, respectively. To obtain numerical results, the numbers of elements for the upper and the lower layer are $N_1 = 67$ and $N_2 = 89$, respectively. For the number of interior points in the upper layer is $M_1 = 361$ and that in the lower layer is the same, $M_2 = 361$.

Using the parameters, elements and interior points described above, numerical results are obtained employing the IDRM presented in the preceding section. To obtain the numerical results, the number of iteration for all of the four cases is 2. There are variations in the values of d for the four different cases. Here, d is the maximum distance between numerical values of K obtained from two consecutive iterations. The criterion for stopping iteration is when the value of d less than $\epsilon = 10^{-4}$. For the case of GL-PCL, the value of d is 0.000015. The value of d for PCL-GL case is 0.000075. The values of d for the cases of PCL-TSL and TSL-PCL are, respectively, 0.000028 and 0.000026, respectively. Some of the results are presented in Figure 2 - Figure 7.

Figure 2 shows soil water potential or suction potential profiles for four different cases, at selected values of X. For more specifically, Figure 2(a) displays the suction potential profile for PCL-GL. In Figure 2(b), the suction potential profile for GL-PCL is presented. The suction potential profile for PCL-TSL is illustrated in Figure 2(c), while Figure 2(d) showcases the suction potential profile for TSL-PCL.

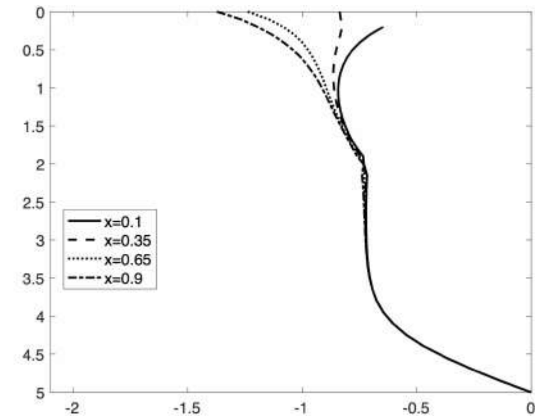

(a) PCL-GL

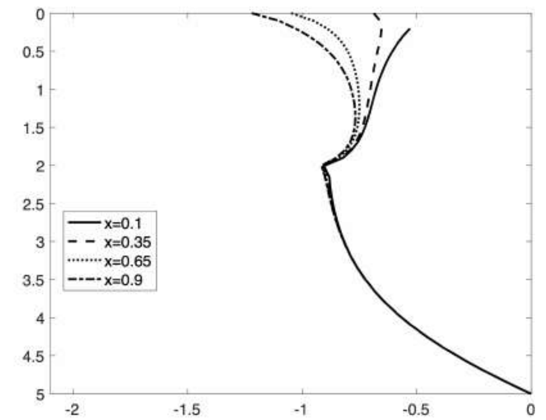

(b) GL-PCL

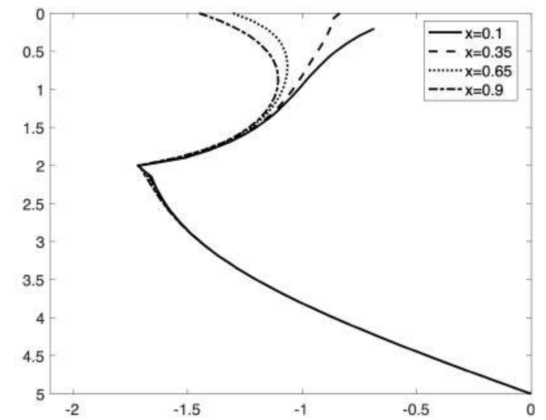

(c) PCL-TSL

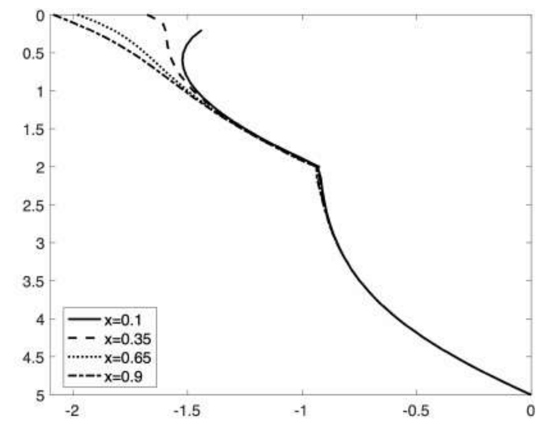

(d) TSL-PCL

Fig. 2: Distribution of suction potential (ψ) at selected values of X.

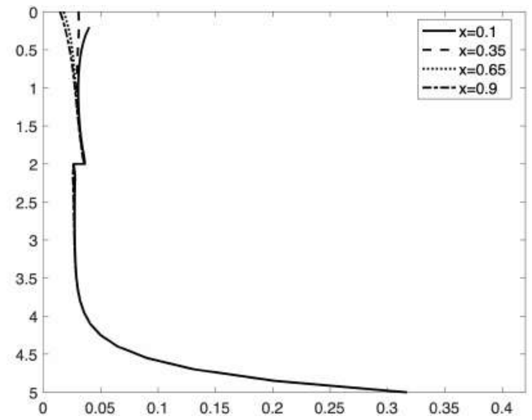

(a) PCL-GL

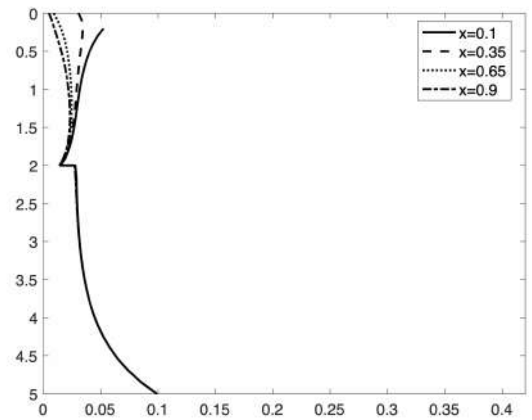

(b) GL-PCL

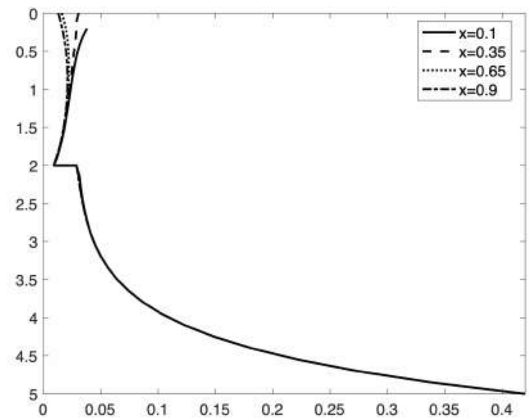

(c) PCL-TSL

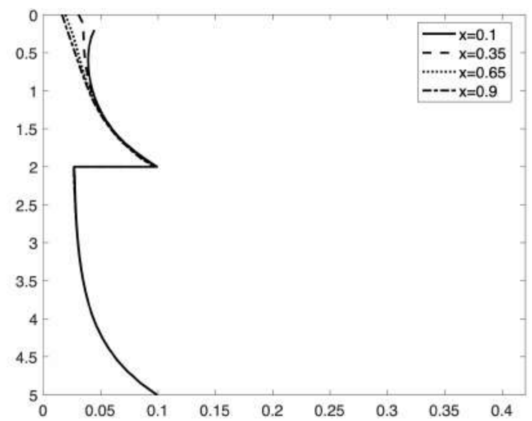

(d) TSL-PCL

Fig. 3: Distribution of hydraulic conductivity (K) at selected values of X.

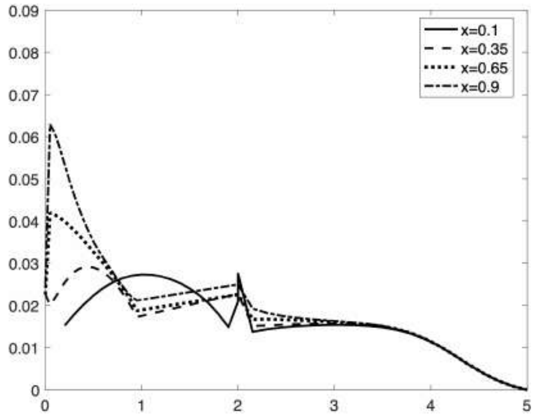

(a) PCL-GL

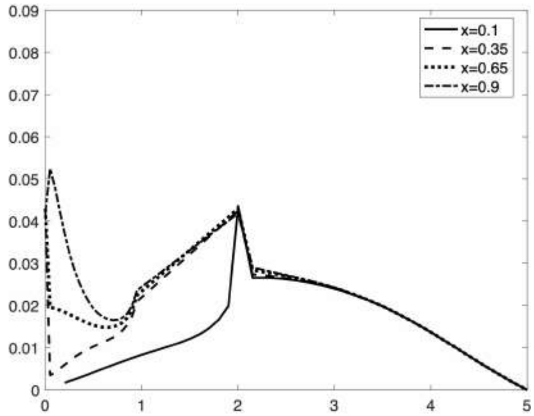

(b) GL-PCL

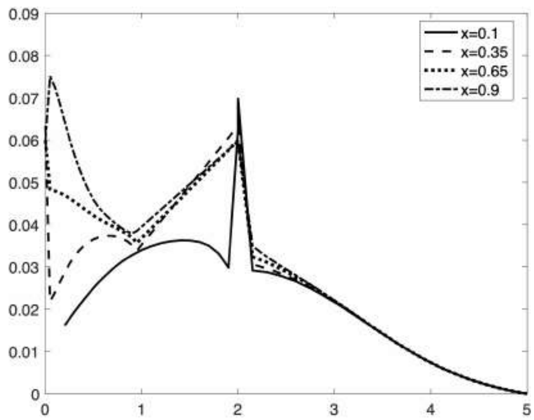

(c) PCL-TSL

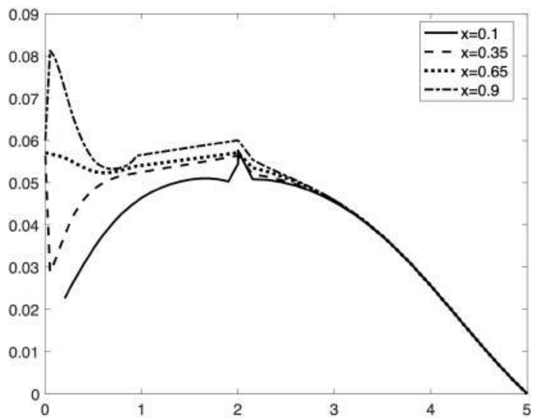

(d) TSL-PCL

Fig. 4: Suction potential (ψ) decrease due to root-water uptake.

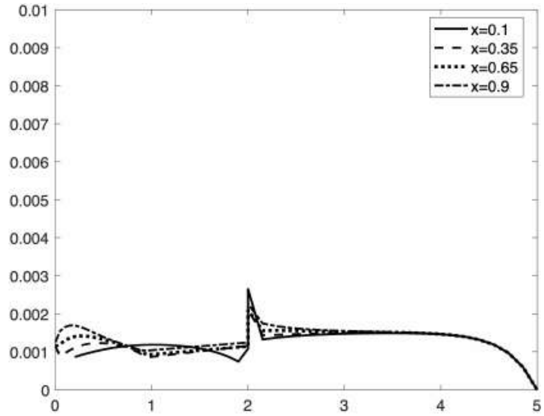

(a) PCL-GL

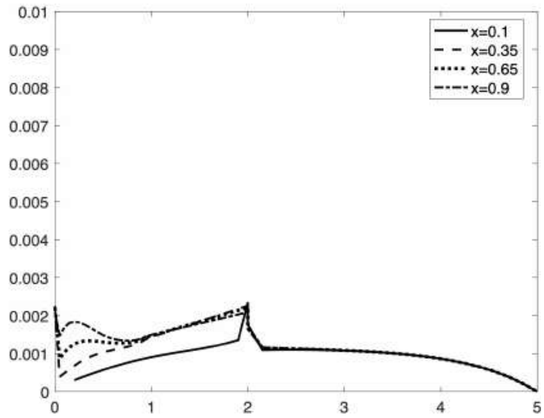

(b) GL-PCL

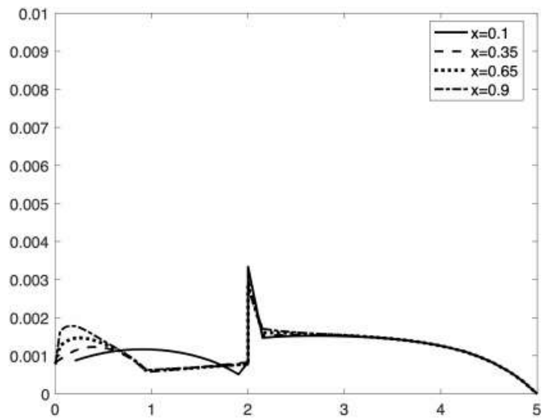

(c) PCL-TSL

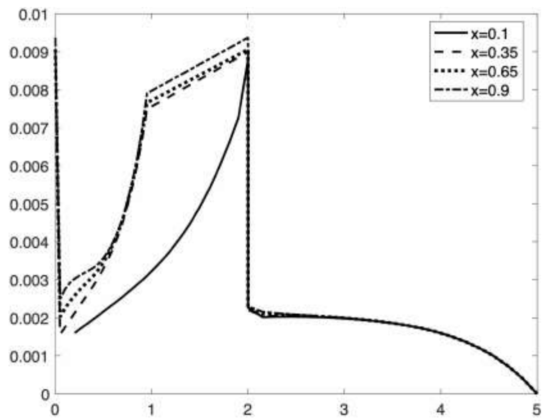

(d) TSL-PCL

Fig. 5: Hydraulic conductivity (K) decrease due to root-water uptake.

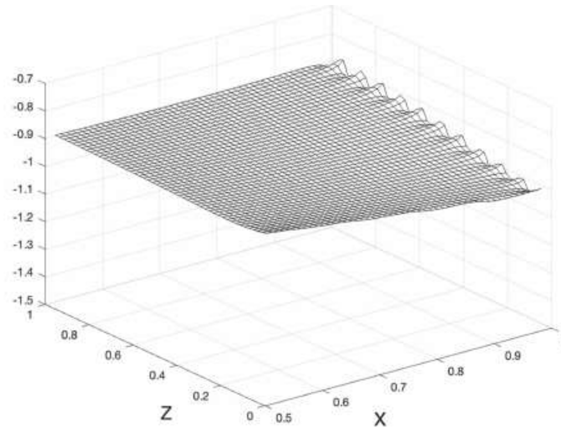

(a) PCL-GL

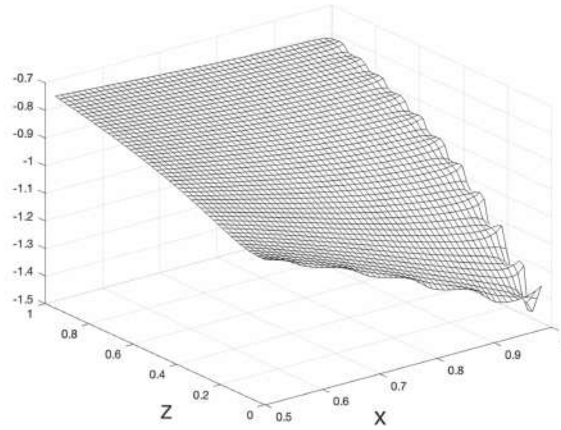

(b) GL-PCL

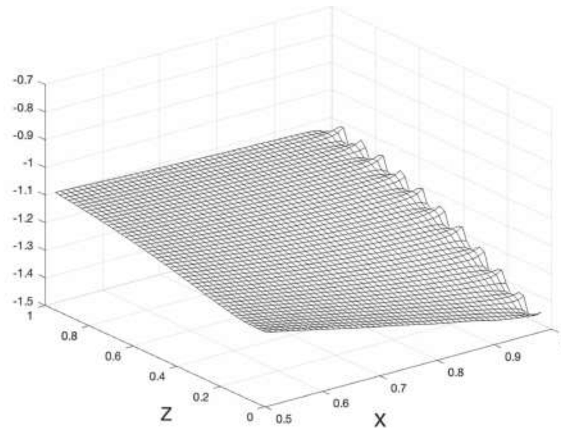

(c) PCL-TSL

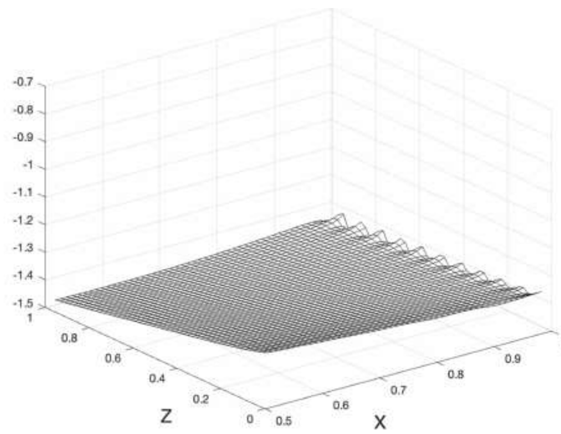

(d) TSL-PCL

Fig. 6: Mesh plots of suction potential over the root zone.

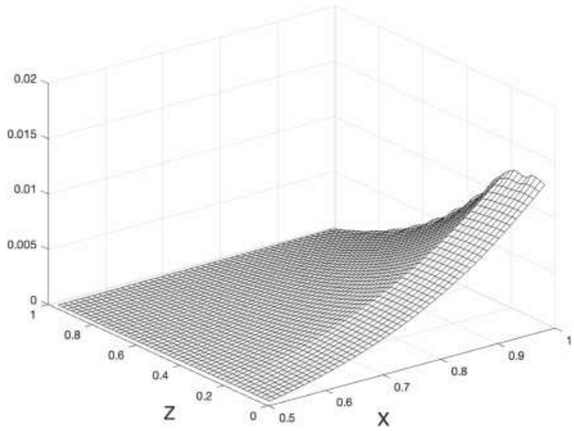

(a) PCL-GL

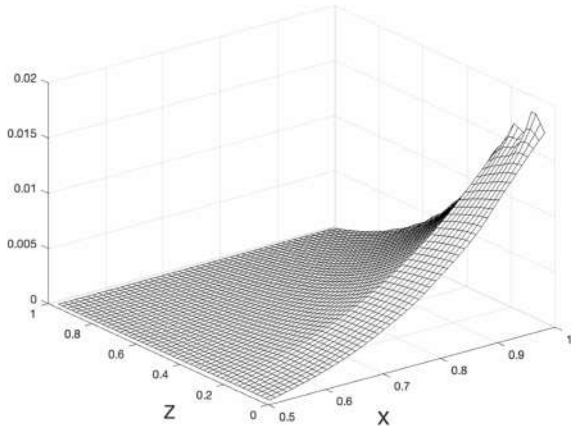

(b) GL-PCL

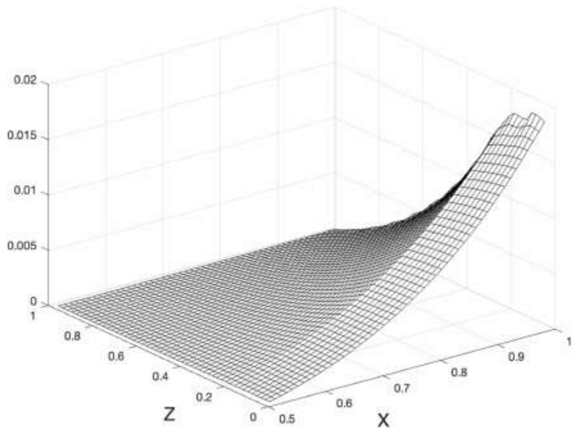

(c) PCL-TSL

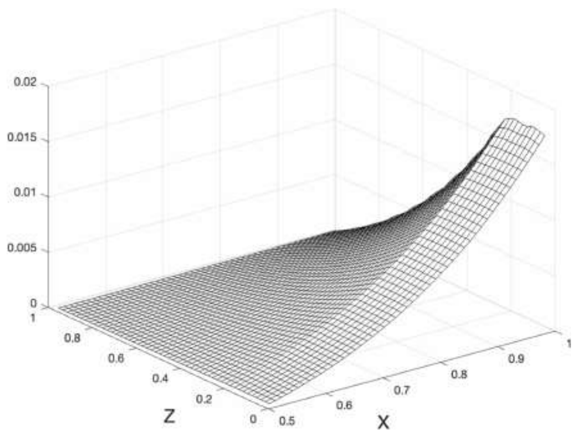

(d) TSL-PCL

Fig. 7: Mesh plots of root-water uptake over the root zone.

As can be seen in Figure 2, variations in the values of ψ are observed in the upper layer. Values of ψ vary from about -1.4 m to -0.5 m at the surface of the upper layer, for PCL-GL and GL-PCL. For PCL-TSL, values of ψ at the surface of the soil are in a range between about -1.4 m and -0.7 m. Values of ψ at the surface of soil fall within a range of between -2.1 m to -1.35 m for TSL-PCL. These results indicate that the soil water potential at the surface of soil is influenced by the soil type of the upper layer. It can also be seen that the suction potential or soil water potential in the upper layer goes to and attain the soil water potential of the lower layer at ψ = 2 m, which is about a constant value.

In the lower layer, for any fixed values of Z, variations in ψ are almost unobserved. The cases of GL-PCL and TSL-PCL have similar distribution of ψ. Values of ψ are in a range of between about -0.9 m and 0. For the case of PCL-GL, ψ is ranged between -0.7 m and 0. Values of ψ for case PCL-TSL are between -1.7 m and 0. These results show that values of ψ in the lower layer depend on the type of the soil in the lower.

Figure 3 shows that the values of K at the surface of soil are determined by the type of soil in the upper layer. For PCL-GL and PCL-TSL, distribution of K at the surface of soil are in similar fashion and ranged between about 0.015 m/day to 0.06 m/day. Values of hydraulic conductivity are in a range of between about 0.01 m/day to 0.07 m/day and 0.02 m/day to 0.065 m/day for GL-PCL and GL-TSL, respectively.

In the lower layer, the distributions of K are driven by the lower layer's soil type. For GL-TSL and PCL-TSL, values of K are between about 0.04 m/day to 0.42 m/day. The range of K is between 0.03 m/day and 0.32 m/day for PCL-GL and TSL-GL, and between 0.03 m/day to 0.1 m/day for GL-PCL and TSL-PCL. On the interface, at $Z = 2$ m, there are jumps in values of K. These results are due to the differences in soil type in the upper layer and the lower layer and the condition of the soil water potential equality at $Z = 2$ m.

Furthermore, the reduction in hydraulic conductivity and suction potential values caused by root-water uptake are presented. The reductions are obtained by subtracting the hydraulic conductivity and the suction potential in this study with the corresponding values of the hydraulic conductivity and the suction potential in [28]. The results are displayed in Figure 4 and Figure 5, respectively.

Figure 4 shows the suction potential decrease due to root-water uptake at the same values of X's in Figure 2. The results show that there are variations in the reduction of ψ, especially at the surface of soil. As can be observed, the highest reduction occurs at $X = 0.9$. This result is expected, as the highest water uptake is at this value of X.

Among the four cases, the highest decrease in ψ occurs in the case of TSL-PCL. The biggest decrease is about 0.08 m. For the case of PCL-TSL, the highest value is about 0.075 m. The highest decrease in ψ for the cases of PCL-GL and GL-PCL are about 0.063 m and 0.053 m, respectively. These results imply that layered soil with TSL results in higher value of the decrease in ψ. This is because when PCL is combined with TSL, the value of ψ at the surface of soil (see Figure 2) lies in the interval -2.1 to -1.3 for TSL-PCL, and -1.4 to -0.6 for PCL-TSL, so that the amount of water uptake is higher than in the other two cases.

Figure 5 shows the decrease in the values of hydraulic conductivity, K, at selected values of X, $X = 0.1, 0.35, 0.65$ and $X = 0.9$, for the four cases considered. As can be seen, the case of TSL-PCL contributes the highest decrease in K. The highest decrease is about 0.0094 m/day, at the surface of soil. The highest decreases for three other cases, PCL-TSL, PCL-GL, and GL-PCL are 0.0037 m/day, 0.0028 m/day, and 0.0025 m/day, respectively. As before, this result is related to the amount of water uptake by the roots, so the order of decreasing of the values of K is the same as the order of decreasing the values of ψ.

Figure 6 shows mesh plots of numerical values of suction potential in the root zone for four different types two-layered soils. Corresponding mesh plots of root uptake are displayed in Figure 7. From Figure 6, it can be seen that for the PCL-GL and TSL-PCL cases, the changes in the value of ψ within the root zone in two cases, namely PCL-GL and TSL-PCL, are not as significant as in the other two cases, namely GL-PCL and PCL-TSL. In the case of PCL-GL, the ψ values are in the range of -1.0 m to -0.9 m. Meanwhile, in the case of TSL-PCL, the ψ values are between -1.47 m and -1.37 m. On the other hand, for the other two cases, significant changes occur in the ψ values. For PCL-TSL, the ψ values are in the range of -1.46 m to -1.1 m, while for GL-PCL, the ψ values are in the range of -1.47 m to -0.8 m.

Based on the ψ distributions in Figure 6 and water stress response function (Equation (4)), the highest root uptake occurs in the GL-PCL and PCL-TSL cases because the ψ values around the point (1.0, 0.2) for both cases reach the highest values. Thus, the distributions of root uptake in these two cases are more or less the same. For the TSL-PCL case, the root uptake distribution is slightly lower compared to the two cases mentioned earlier, and the distribution of root uptake is also more or less the same as those two cases. Meanwhile, for the PCL-GL case, because the ψ distribution is higher than the other three cases, its root uptake distribution is lower than the three previous cases.

Furthermore, the total water uptake (TWU) is numerically calculated. The root zone is subdivided into 50×50 equal regions. Let (X_{ij}, Z_{ij}) denote the coordinates of the top-right corner of the region in the i-th row and j-th column. The TWU is computed using the following formula.

$$TWU = \sum_{i=1}^{50} \sum_{j=1}^{50} S(X_{ij}, Z_{ij}, \psi_{ij}). \qquad (39)$$

Here ψ_{ij} represents the suction potential at the top-right corner of the i-th row and j-th column. The results obtained using Equation (39) are summarized in Table III.

TABLE III: Total water uptake from different types of layered soils.

	PCL-GL	GL-PCL	PCL-TSL	TSL-PCL
Total uptake (cm^3/day)	1140.12	1320.69	1553.42	1660.79

From Table III, it can be seen that TSL-PCL results in highest value of TWU compared to other two-layered soils. This result is due to the fact that the values of ψ in this case lies between -1.4 and -1.5, which is the smallest compared to the other cases, as shown in Figure 6. From Equation (4), these values of ψ result in the highest values of $\gamma(\psi)$. As a consequence, they also yield the highest values of TWU. Using the same reasoning, the other results in Table III can be obtained from the results in Figure 6.

V. Concluding remarks

A mathematical model has been developed to describe the steady infiltration process from periodic trapezoidal channels into soils with two distinct layers, taking into account root-water uptake. This model has been effectively solved through numerical techniques, employing an Iterative Dual Reciprocity Method (IDRM). Using the IDRM, we have obtained numerical solutions for hydraulic conductivity and computed numerical values for soil water potential. To assess the method's performance, we have conducted tests on four different problems.

The findings from our analysis reveal that the hydraulic conductivity and soil water potential in the lower layer are primarily influenced by the properties of the soil in that lower layer. Conversely, at the surface of the upper soil layer, these parameter values are predominantly influenced by the type of soil in this layer. Furthermore, the values of these parameters go towards the values of the corresponding parameters at the top of the lower layer. Furthermore, the smallest suction potential at the soil surface leads to the highest total water uptake.

References

[1] Srinita SA, Nielsen DR, Kirkham D. Steady flow of water through a two-layer soil, Water Resour. Res. 1969; 5(5): 1053 - 1063.

[2] Srivastava R, Yeh TCJ. Analytical solution for one-dimensional, transient infiltration toward the water table in homogeneous and layered soils. Water Resour. Res. 1991; 27(5): 753 - 762.

[3] Barontini S, Ranzi R, Bacchi B. Water dynamics in a gradually nonhomogeneous soil described by linearized Richards equation. Water Resour. Res. 2007; 43(8): W08411.

[4] De Luca DL, Cepeda JM. Procedure to obtain analytical solutions of one-dimensional Richard's equation for infiltration in two-layered soils. Journal of Hydrologic Engineering. 2016; 21(7): 04016018-1 - 04016018-11.

[5] Oldenburg CM, Pruess K. On numerical modeling of capillary barriers. Water Resour. Res. 1993; 29(4): 1045 - 1056.

[6] Ross PJ, Bristow KL. Simulating water movement in layered and gradational soils using the Kirchhoff transform. Soil Sci. Soc. Am. J. 1990; 54(6): 1519 - 1524.

[7] Walter MT, Kim JS, Steenhuis TS, Parlange JY, Heilig A, Braddock RD, Selker JS, Boll J. Funneled flow mechanisms in a sloping layered soil: Laboratory investigation. Water Resour. Res. 2000; 36(4): 841 - 849.

[8] Belfort B, Lehmann F. Comparison of equivalent conductivities for numerical simulation of one-dimensional unsaturated flow. Vadoze Zone J. 2005; 4(4): 1191 - 1200.

[9] Brunone B, Ferrante M, Romano N, Santini A. Numerical simulations of one-dimensional infiltration into layered soils with the Richard's equation using different estimates of the interlayer conductivity. Vadoze Zone Journal. 2003; 2(2): 193 - 200.

[10] Celia M, Bouloutas E, Zarba R. A general mass-conservative numerical solution for the unsaturated flow equation. Water Resour. Res. 1990; 26(7); 1483 - 1496.

[11] Haverkamp R, Vauclin M. A note on estimating finite difference interblock hydraulic conductivity values for transient unsaturated flow problems. Water Resour. Res. 1979; 15: 181 - 187.

[12] Li H, Farthing M, Dawson C, Miller CT. Local discontinouos Galerkin approximations to Richards equation. Adv. Water Resour. 2007; 30(3); 555 - 575.

[13] Li H, Farthing M, Miller CT. Adaptive local discontinouos Galerkin approximations to Richards equation. Adv. Water Resour. 2007; 30(9); 1883 - 1901.

[14] Lima-Vivancos V, Voller V. Two numerical methods for modelling variably saturated flow in layered media. Vadose Zone J. 2004; 3(3): 1031 - 1037.

[15] Pall R, Jarret AR, Morrow CT. Transient soil moisture movement through layered soils using a finite element approach. Transactions of the ASAE. 1981; 24(3): 678 - 683.

[16] van Dam J, Feddes R. Numerical simulation of infiltration, evaporation and shallow groundwater levels with the Richards equation. J. Hydrol. 2000; 233(1); 72 - 85.

[17] Diaw EB, Lehmann F, Ackerer Ph. One-dimensional simulation of solute transfer in saturated–unsaturated porous media using the discontinuous finite elements method. Journal of Contaminant Hydrology. 2001; 51(3-4): 197 - 213.

[18] Farthing MW, Kees CE, Miller CT. Mixed finite element methods and higher-order temporal approximations. Advances in Water Resources. 2002; 25(1): 85 - 101.

[19] Matthews CJ, Braddock RD, Sander GC. Modeling flow through a one-dimensional multi-layered soil profile using the method of lines. Environmental Modeling and Assessment 2004; 9: 103 - 113.

[20] Katsikadelis JT. Boundary elements: Theory and applications. Elsevier, Amsterdam-London-New York-Oxford-Paris-Tokyo-Boston-San Diego-San Francisco-Singapore-Sydney, 2002.

[21] Zhu S, Satravaha P. An efficient computational method for modelling transient heat conduction with nonlinear source terms. Applied Mathematical Modelling. 1996; 20(7): 513 - 522.

[22] Clements DL, Lobo M. A BEM for time dependent infiltration from an irrigation channel. Eng. Anal. Bound. Elem. 2010; 34(12): 1100 - 1104.

[23] Lobo M, Clements DL, Widana N. Infiltration from irrigation channels into soil with impermeable inclusions. ANZIAM J. 2005; 46(E): C1005 - C1068.

[24] Solekhudin I, Ang KC, A DRBEM with a predictor–corrector scheme for steady infiltration from periodic channels with root-water uptake. Eng. Anal. Bound. Elem. 2012; 36: 1199 - 1204.

[25] Solekhudin I, Ang KC, A DRBEM for time-dependent infiltration from periodic irrigation channels in a homogeneous soil. Electronic Journal of Bound. Elem. 2013; 11(1): 1 - 12.

[26] Solekhudin I, Ang KC, A Laplace transform DRBEM with a predictor–corrector scheme for time-dependent infiltration from periodic channels with root-water uptake. Eng. Anal. Bound. Elem. 2015; 50: 141 - 147.

[27] Solekhudin I. A numerical method for time-dependent infiltration from periodic trapezoidal channels with different types of root-water uptake. IAENG International Journal of Applied Mathematics. 2018; 48(1): 84 - 89.

[28] Solekhudin I. Boundary interface water infiltration into layered soils using dual reciprocity methods. Engineering Analysis with Boundary Elements. 2020; 119: 280 - 292.

[29] Azis MI, Clements DL, Lobo M. A boundary element method for steady infiltration from periodic channels. ANZIAM J. 2003; 44(E): C61 – C78.

[30] Philip JR. Flow in porous media. Annu. Rev. Fluid Mech. 1970; 2: 177 - 204.

[31] Philip JR. The scattering analog for infiltration in porous media. Rev. of Geophysics. 1989; 27(4): 431 - 448.

[32] Philip JR. Steady infiltration from circular cylindrical cavities. Soil Science Society of America Journal. 1984; 48(2): 270 - 278.

[33] Pullan AJ. Linearized time-dependent infiltration from a shallow pond. Water Resour. Res. 1992; 28(4): 1041 - 1046.

[34] Waechter RT, Philip JR. Steady two- and three-dimensional flows in unsaturated soil: the scattering analog. Water Resour. Res. 1985; 21(12): 1875 - 1887.

[35] Basha HA. Multidimensional linearized nonsteady infiltration with prescribed boundary conditions at the soil surface, Water Resour. Res. 1999; 35(1): 75 - 83.

[36] Farthing MW, Ogden FL. Numerical solution of Richards' equation: A review of advances and challenges. Soil Sci. Soc. Am. J. 2017; 81: 1257 – 1269.

[37] List F, Radu FA. A study on iterative methods for solving Richards' equation. Comput. Geosci. 2016; 20: 341 – 353.

[38] Wever N, Fierz C, Mitterer C, Hirashima H, Lehning M. Solving Richards equation for snow improves snowpack meltwater runoff estimations in detailed multi-layer snowpack model. The Cryosphere. 2014; 8: 257 - 274.

[39] Batu V. Steady infiltration from single and periodic strip sources. Soil Sci. Soc. Am. J. 1978; 42: 544 - 549.

[40] Li KY, De-Jong R, Boisvert JB. An exponential root-water uptake model with water stress compensation. Journal of Hydrology. 2001; 252: 189 - 204.

[41] Peters A, Durner W, Idenb SC. Modified Feddes type stress reduction function for modeling root water uptake: Accounting for limited aeration and low water potential. Agricultural Water Management 2017; 185: 126 – 136.

[42] Gardner WR. Some steady-state solutions to the unsaturated moisture flow equation with application to evaporation from a water table. Soil Sci. 1958; 85: 228 - 232.

[43] Waechter RT, Mandal AC. Steady Infiltration From a Semicircular Cylindrical Trench and a Hemispherical Pond Into Unsaturated Soil. Water Resour. Res. 1993; 29(2): 457 - 467.

[44] Basha HA. Multidimensional linearized nonsteady infiltration toward a shallow water table, Water Resour. Res. 2000; 36(9): 2567 - 2573.

[45] Amoozegar-Fard A, Warrick AW, Lomen DO. Design nomographs for trickle irrigation system. J. Irrig. Drain. Eng. 1984; 110: 107 - 120.

[46] Bresler E. Analysis of trickle irrigation with application to design problems, Irrigation Science. 1978; 1: 3 - 17.

[47] Vrugt JA, Hopmans JW, Simunek. Calibration of a Two-Dimensional Root Water Uptake Model. Soil Sci. Soc. Am. J. 2001; 65: 1027 - 1037.